Lattice computations of the pion form factor

Frederic D. R. Bonnet,[1,2,*] Robert G. Edwards,[2,†] George T. Fleming,[2,3,‡] Randy Lewis,[1,§] and David G. Richards[2,‖]

[1]*Department of Physics, University of Regina, Regina, SK, S4S 0A2, Canada*
[2]*Thomas Jefferson National Accelerator Facility, Newport News, Virginia 23606, USA*
[3]*Sloane Physics Laboratory, Yale University, New Haven, Connecticut 06520, USA*

(Received 27 November 2004; published 12 September 2005)

We report on a program to compute the electromagnetic form factors of mesons. We discuss the techniques used to compute the pion form factor and present results computed with domain-wall valence fermions on MILC ASQTAD lattices, as well as with Wilson fermions on quenched lattices. We find that the full-QCD form factor is well described by a VMD picture, with the pole mass in the chiral limit $m_{\mathrm{VMD}} = 0.868(65)$ GeV. However, the quenched Wilson fermion results are suggestive of large scaling violations.

DOI: 10.1103/PhysRevD.72.054506 PACS numbers: 13.40.Gp, 14.40.Aq, 12.38.Gc

I. INTRODUCTION

The pion electromagnetic form factor is often considered a good observable for studying the onset, with increasing energy, of the perturbative QCD (pQCD) regime for exclusive processes. It is believed that, because the pion is the lightest and simplest hadron, a perturbative description will be valid at lower energy scales than predictions for heavier and more complicated hadrons such as the nucleon [1].

A pseudoscalar particle has only a single electromagnetic form factor, $F(Q^2)$, where Q^2 is the four-momentum transfer, and furthermore at $Q^2 = 0$, this form factor is normalized to the electric charge of the particle, $F(Q^2 = 0) = 1$; the magnetic form factor vanishes. Thus, in this paper, we will be measuring the form factor of the positively charged π^+. The experimentally observed behavior of the form factor at small-momentum transfer is well described by the vector-meson-dominance (VMD) hypothesis [2–4]

$$F_\pi(Q^2) \approx \frac{1}{1 + Q^2/m^2_{\mathrm{VMD}}} \quad \text{for } Q^2 \ll m^2_{\mathrm{VMD}}. \qquad (1)$$

The current experimental situation is presented in Fig. 1.

For $Q^2 \leq 0.28$ GeV^2, Amendolia *et al.* [5] have determined the form factor to high precision from scattering of very high energy pions upon atomic electrons in a fixed target. For higher Q^2, the form factor has been determined from quasielastic scattering from a virtual pion in the proton [6–8]. In this case, the extracted values for the form factor must depend upon some theoretical model [9–11] for extrapolating the observed scattering from virtual pions to the expected scattering from on-shell pions. As the models have become more sophisticated, the earlier data [6,7] have been reanalyzed [12] for consistency. Shown in Fig. 1 are the results of some model calculations which seem to cover the range of existing predictions [13–16].

Given the dominance of the rho meson resonance in the timelike region ($Q^2 < 0$) of the pion form factor, perhaps it is not too surprising that the spacelike form factor is well described at low $Q^2 > 0$ by a VMD-inspired monopole form with only a contribution from the lightest vector resonance ($m_{\mathrm{VMD}} \sim m_\rho \approx 0.77$ GeV). What is striking is that it accurately describes all experimental data even up to scales of $Q^2 \gtrsim 1$ GeV^2. Furthermore, VMD predicts that the form factor should scale as $F_\pi(Q^2) \sim 1/Q^2$ for $Q^2 \gg m^2_{\mathrm{VMD}}$, the same scaling predicted at asymptotically high Q^2 in perturbative QCD [17,18]. One crucial fact which makes the pion form factor an ideal observable for studying the interplay between perturbative and nonperturbative QCD is that its asymptotic normalization can be determined from pion decay [19–25]

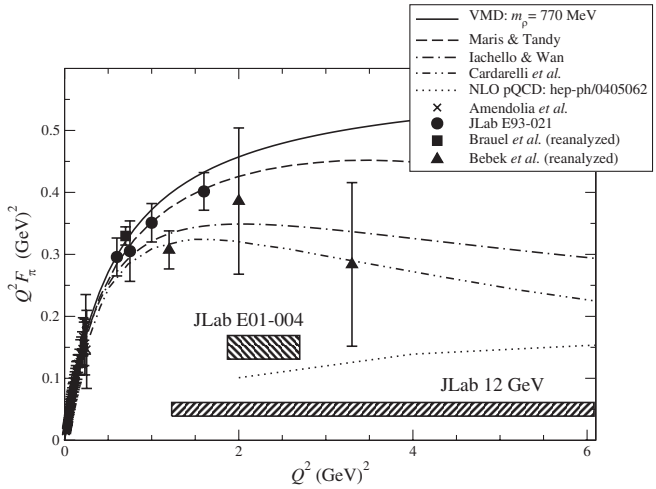

FIG. 1. Summary of experimental data for the pion electromagnetic form factor; shaded regions indicate expected sensitivities and coverage of future results. The lines indicate theoretical calculations of the form factor, as described in the text.

*Electronic address: fbonnet@jlab.org
†Electronic address: edwards@jlab.org
‡Electronic address: George.Fleming@Yale.edu
§Electronic address: Randy.Lewis@uregina.ca
‖Electronic address: dgr@jlab.org

$$F_\pi(Q^2) = \frac{8\pi\alpha_s(Q^2)f_\pi^2}{Q^2} \quad \text{as} \quad Q^2 \to \infty. \tag{2}$$

Higher order perturbative calculations of the hard contribution to the form factor [26–29] do not vary significantly from this value, and are shown in Fig. 1. At the largest energy scale where reliable experimental measurements have so far been obtained, around $Q^2 \simeq 2$ GeV^2, the data are 100% larger than this pQCD asymptotic prediction. However, an improved choice of strong-interaction scale improves this picture considerably[30].

This situation raises many questions. At what scale does the form factor vary with Q^2 as predicted by pQCD? However, merely observing the proper Q^2 dependence is insufficient as Eq. (1) has the same asymptotic Q^2 dependence as pQCD but is numerically about twice as large. How rapidly will the data approach the pQCD prediction and at what scale will pQCD finally agree with the data? These are questions which lattice QCD calculations are ideally suited to address, provided we can get reliable results for momentum transfer on the order of a few to several GeV^2.

Early lattice calculations validated the vector-meson-dominance hypothesis at low Q^2 [31,32]. Recent lattice results [33–38], including some of our own preliminary results [39,40], have somewhat extended the range of momentum transfer, up to 2 GeV^2, and the results remain consistent with VMD and the experimental data.

II. LATTICE COMPUTATION OF $F_\pi(Q^2)$

The electromagnetic form factor is obtained in lattice QCD simulations by placing a charged pion creation operator at Euclidean time t_i, a charged pion annihilation operator at t_f, and a vector current insertion at t as shown in Fig. 2. A standard quark propagator calculation provides the two propagator lines that originate from t_i. The remaining quark propagator, originating from t_f is obtained via the *sequential source method*: (1) completely specify the quantum numbers, including momentum $\boldsymbol{p}_f$, of the annihilation operator to be placed at t_f and (2) contract the propagator from t_i to t_f to the annihilation operator and use that product as the source vector of a second, sequential propagator inversion. The resulting sequential propagator

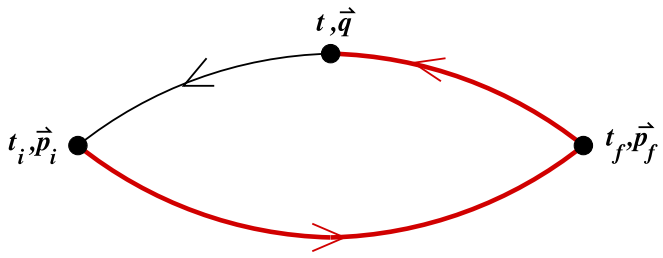

FIG. 2 (color online). The quark propagators used to compute the pion form factor.

appears as the thick line in Fig. 2 extending from t_i to t via t_f. Given these two propagators, the diagram can be computed for all possible values of insertion position t and insertion momenta $\boldsymbol{q}$; the initial momentum $\boldsymbol{p}_i$ is determined by momentum conservation $\boldsymbol{p}_i = \boldsymbol{p}_f - \boldsymbol{q}$.

Furthermore, with the same set of propagators, any current can be inserted at t and any meson creation operator can be contracted at t_i. So, the diagram relevant to determining the form factor for the transition $\rho^+ \to \gamma^*\pi^+$ can be computed without further quark propagator calculations. By applying the sequential source method at the sink, the trade-off is that the entire set of sequential propagators must be recomputed each time new quantum numbers are needed at the sink, particularly $\boldsymbol{p}_f$.

We can extract the pion energies $E_\pi(\boldsymbol{p})$ using standard lattice techniques of fitting pion correlation functions from which we can compute the momentum transfer

$$-Q^2 = [E_\pi(\boldsymbol{p}_f) - E_\pi(\boldsymbol{p}_i)]^2 - (\boldsymbol{p}_f - \boldsymbol{p}_i)^2 \tag{3}$$

which should be nonpositive if the pion spectral function is well behaved. Since the largest Q^2 for a given $|\boldsymbol{p}|^2$ occurs in the Breit frame, $\boldsymbol{p}_f = -\boldsymbol{p}_i$, it is important to choose a nonzero $\boldsymbol{p}_f$ to achieve large momentum transfer; indeed $\boldsymbol{p}_f = 0$ yields a vanishing Q^2 for all $\boldsymbol{q}$ in the chiral limit.

The form factor, $F(Q^2)$, is defined by

$$\begin{aligned}\langle\pi(\boldsymbol{p}_f)|V_\mu(0)|\pi(\boldsymbol{p}_i)\rangle_{\text{continuum}} &= Z_V\langle\pi(\boldsymbol{p}_f)|V_\mu^{\text{lat}}(0)|\pi(\boldsymbol{p}_i)\rangle \\ &= F(Q^2)(p_i + p_f)_\mu \end{aligned}\tag{4}$$

where $V_\mu^{\text{lat}}(x)$ is a particular lattice discretization of the continuum vector current, and Z_V is the corresponding matching factor relating the lattice current to that in the continuum. In this work we use the local and point-split currents, $V_\mu^{\text{loc}}(x)$ and $V_\mu^{\text{p.s.}}(x)$, defined by

$$V_\mu^{\text{loc}}(x) = \overline{\psi}(x)\gamma_\mu\psi(x), \tag{5}$$

$$\begin{aligned}V_\mu^{\text{p.s.}}(x) = \frac{1}{2}\{&\overline{\psi}(x+\hat{\mu})U_\mu^\dagger(x)[1+\gamma_\mu]\psi(x) \\ &- \overline{\psi}(x)U_\mu(x)[1-\gamma_\mu]\psi(x+\hat{\mu})\}.\end{aligned}\tag{6}$$

In the case of the Wilson action, the point-split current is conserved, i.e. $Z_V^{\text{p.s.}} = 1$. While this current is no longer conserved with the domain-wall fermion (DWF) action, the two currents mix with different operators at $\mathcal{O}(a^2)$, and therefore are subject to different discretization errors for $Q^2 \neq 0$. Thus, their use should allow some indication of discretization uncertainties.

To determine the form factor, we compute the three-point correlation function depicted in Fig. 2, given by

$$\begin{aligned}\Gamma^{AB}_{\pi\mu\pi}(t_i, t, t_f, \boldsymbol{p}_i, \boldsymbol{p}_f) = \sum_{\boldsymbol{x}i\boldsymbol{x}_f}, e_f^{-i(\boldsymbol{x}_f-\boldsymbol{x})\cdot\boldsymbol{p}_f} e^{-i(\boldsymbol{x}-\boldsymbol{x}_i)\cdot\boldsymbol{p}_i} \\ \times\langle 0|\phi_B(x_f)V_\mu(x)\phi_A^\dagger(x_i)|0\rangle\end{aligned}\tag{7}$$

where $\phi_A^\dagger(x)$ and $\phi_B(x)$ are creation and annihilation operators with pion quantum numbers. The A and B indicate that different operators may be used at the source and sink, i.e. smeared source and point sink or pseudoscalar source and axial-vector sink.

Inserting complete sets of hadron states, and requiring $t_i \ll t \ll t_f$, gives

$$\Gamma^{AB}_{\pi\mu\pi}(t_i, t, t_f, \boldsymbol{p}_i, \boldsymbol{p}_f) \rightarrow \langle 0|\phi_B(0)|\pi(\boldsymbol{p}_f)\rangle \frac{e_f^{-(t_f-t)E_\pi(\boldsymbol{p}_f)}}{2E_\pi(\boldsymbol{p}_f)} \times \langle \pi(\boldsymbol{p}_f)|V_\mu(0)|\pi(\boldsymbol{p}_i)\rangle \times \frac{e_i^{-(t-t_i)E_\pi(\boldsymbol{p}_i)}}{2E_\pi(\boldsymbol{p}_i)} \langle \pi(\boldsymbol{p}_i)|\phi_A^\dagger(0)|0\rangle. \tag{8}$$

Similarly for the two-point correlator, with $t_i \ll t_f$,

$$\Gamma^{AB}_{\pi\pi}(t_i, t_f, \boldsymbol{p}) \rightarrow \langle 0|\phi_B(0)|\pi(\boldsymbol{p})\rangle \frac{e^{-(t_f-t_i)E_\pi(\boldsymbol{p})}}{2E_\pi(\boldsymbol{p})} \times \langle \pi(\boldsymbol{p})|\phi_A^\dagger(0)|0\rangle. \tag{9}$$

We use both the pseudoscalar density, $\phi^{(1)}(x) = \overline{\psi}(x)\gamma_5\psi(x)$, and the temporal component of the axial-vector current, $\phi^{(2)}(x) = \overline{\psi}(x)\gamma_5\gamma_4\psi(x)$, as pion interpolating operators, constructed from both local and smeared quark fields, denoted by L and S, respectively. We adopt gauge-invariant Gaussian smearing

$$b(x) \rightarrow \left(1 + \frac{\omega}{N}\boldsymbol{\nabla} U\right)^N b(x), \tag{10}$$

where ω and N are the tunable parameters used to specify the smearing radius; the flavor structure is suppressed. The respective merits of these interpolating operators will be discussed later. For these operators, we define the following amplitudes:

$$\langle 0|\phi_L^{(1)}(0)|\pi(\boldsymbol{p})\rangle = Z_L^{(1)}, \tag{11}$$

$$\langle 0|\phi_S^{(1)}(0)|\pi(\boldsymbol{p})\rangle = Z_S^{(1)}(|\boldsymbol{p}|), \tag{12}$$

$$\langle 0|\phi_L^{(2)}(0)|\pi(\boldsymbol{p})\rangle = Z_L^{(2)}(|\boldsymbol{p}|), \tag{13}$$

$$\langle 0|\phi_S^{(2)}(0)|\pi(\boldsymbol{p})\rangle = Z_S^{(2)}(|\boldsymbol{p}|). \tag{14}$$

The overlap of the operator $\phi_L^{(2)}$ has trivial $\boldsymbol{p}$ dependence arising from the Lorentz structure of the operator

$$Z_L^{(2)} = E(|\boldsymbol{p}|) f_\pi. \tag{15}$$

However, the introduction of an additional three-dimensional scale introduces nontrivial $\boldsymbol{p}$ dependence for the smeared overlaps $Z_S^{(1)}$ and $Z_S^{(2)}$.

We employ two methods to determine the form factor $F_\pi(Q^2)$. The first method, which we call the *fitting method*, involves a fit of the relevant two- and three-point functions to simultaneously extract the form factor, the energies $E_\pi(\boldsymbol{p})$, and the amplitudes $Z(\boldsymbol{p})$ in a single covariant, jackknifed fit.

The second method, which we call the *ratio method*, starts by determining the energies $E_\pi(\boldsymbol{p})$, either by fits to the correlators at nonzero momentum or from a dispersion relation, and then constructing the following ratio which is independent of $Z_L^{(1)}$, $Z_S(|\boldsymbol{p}|)$, and all Euclidean time exponentials for sufficiently large temporal separations:

$$F(Q^2, t) = \frac{\Gamma^{AB}_{\pi 4\pi}(t_i, t, t_f, \boldsymbol{p}_i, \boldsymbol{p}_f)\Gamma^{CL}_{\pi\pi}(t_i, t, \boldsymbol{p}_f)}{\Gamma^{AL}_{\pi\pi}(t_i, t, \boldsymbol{p}_i)\Gamma^{CB}_{\pi\pi}(t_i, t_f, \boldsymbol{p}_f)} \times \left(\frac{2Z_V E_\pi(\boldsymbol{p}_f)}{E_\pi(\boldsymbol{p}_i) + E_\pi(\boldsymbol{p}_f)}\right) \tag{16}$$

where the indices A, B, and C can be either L (local) or S (smeared). As part of our program, we expect to determine the relative merits of each extraction method. Furthermore, excited states have different contributions in the two methods.

Since the form factor is absolutely normalized at zero momentum transfer, $F(Q^2 = 0) = 1$, a precise computation of Z_V for each of our chosen currents can be obtained by applying Eq. (16) for $\boldsymbol{p}_i = \boldsymbol{p}_f$:

$$Z_V = \frac{\Gamma^{AB}_{\pi\pi}(t_i, t_f, \boldsymbol{p}_i)}{\Gamma^{AB}_{\pi 4\pi}(t_i, t, t_f, \boldsymbol{p}_i, \boldsymbol{p}_f)}. \tag{17}$$

III. SIMULATION DETAILS

Our first calculations were performed on quenched configurations generated with the Wilson gauge action at inverse coupling $\beta = 6.0$, corresponding to $a^{-1} \approx 2$ GeV. The propagators were computed using the unimproved Wilson fermion action with Dirichlet boundary conditions in the temporal direction, and periodic boundary conditions in the spatial directions. For Wilson fermions at these lattice spacings, the exceptional configuration problem is rather mild, particularly when compared to that for the nonperturbatively improved clover action. This enabled us to reach pion masses of 300 MeV without observing any exceptional configurations, whereas computations using the clover action are limited to pion masses in excess of roughly 360 MeV [33,36] due to the systematic errors caused by the frequent occurrence of exceptional configurations. A detailed listing of the simulation parameters is provided in Table I.

The pion masses attainable in quenched DWF calculations are limited only by finite volume effects and available computing power. So far, however, quenched DWF computations of the pion form factor have only explored pion masses down to 390 MeV, at $a^{-1} \approx 1.3$ GeV [34]. An important advantage of DWF fermions is that they are automatically $\mathcal{O}(a)$ improved. An alternative approach

TABLE I. Simulation details for quenched Wilson fermion calculations at $a^{-1} \approx 2$ GeV.

κ	Volume	am_ρ	am_π	m_π/m_ρ	$m_\pi L$	Z_V^{loc}
0.1480	$16^3 \times 32$	0.7187(39)	0.6752(45)	0.943(10)	10.80(7)	0.82725(51)
0.1500	$16^3 \times 32$	0.6387(57)	0.5854(45)	0.900(13)	9.36(7)	0.78486(46)
0.1520	$16^3 \times 32$	0.5540(83)	0.4851(67)	0.876(14)	7.76(11)	0.74197(54)
0.1540	$16^3 \times 32$	0.4682(124)	0.3752(73)	0.801(23)	6.00(11)	0.70459(39)
0.1555	$24^3 \times 32$	0.4209(88)	0.2613(29)	0.621(14)	6.27(7)	$\cdots$
0.1563	$24^3 \times 32$	0.4014(68)	0.1921(29)	0.479(10)	4.61(7)	0.65676(43)
0.1566	$32^3 \times 48$	0.3724(145)	0.1629(36)	0.437(19)	5.21(12)	0.65553(14)

using twisted-mass QCD (tmQCD), in which Wilson fermion results are also $\mathcal{O}(a)$ improved with just double the effort [41], has been explored separately [35].

The Lattice Hadron Physics Collaboration (LHPC) has been employing the MILC Collaboration's $N_f = 2 + 1$ and $N_f = 3$ configurations generated with staggered ASQTAD sea quarks[42] to perform unquenched hadron structure calculations [43–47]. Valence propagators are then computed using a domain-wall fermion action:

$$S_{\mathrm{DWF}} = -\sum_i^{L_s} \bar{\Psi}_i \{[D_{\mathrm{W}}(-M) + 1]\Psi_i - P_- \Psi_{i+1} - P_+ \Psi_{i-1}\}, \tag{18}$$

where $D_{\mathrm{W}}(M)$ is the standard Wilson kernel with mass M, L_s is the extent of the lattice in the fifth dimension, and the fermion fields satisfy the boundary conditions

$$P_- \Psi_{L_s+1} = -mP_- \Psi_1, \qquad P_+ \Psi_0 = -mP_+ \Psi_{L_s},$$

with chiral projection operators $P_\pm = \frac{1}{2}(1 \pm \gamma_5)$. In this work, we employed a domain-wall height $M = 1.7$, and spatial extent $L_s = 16$. The MILC configurations were hypercubic blocked [48] before the valence propagators were computed to avoid unacceptably large residual chiral symmetry breaking, and the propagators were computed with Dirichlet boundaries to $t = 0$ and $t = 32$, one half of the temporal extent of the lattices, to save computational effort. The simulation parameters for the DWF computation are provided in Table II. A detailed study of the physical properties of light hadrons composed of staggered quarks computed on these lattices has recently been completed by the MILC Collaboration [49]. We use their determinations of the lattice spacings through the 2S-1S and 1P-1S splitting in Υ to express our results in physical units.

IV. RESULTS

The pion form factor for the quenched Wilson case is obtained by applying the fitting method to the conserved, point-split vector current $V_\mu^{\mathrm{p.s.}}$. For most of our Wilson data, we have also computed the form factor using the local vector current, and for this data we show the corresponding matching factors Z_V^{loc} in Table I; the determination using the two currents is consistent. Our results at each value of κ are shown in Fig. 3. Also indicated is the VMD form using the experimental value for the ρ meson mass, together with recent experimental data, illustrating the extent to which VMD describes the data.

While the lattice data tend in the correct direction with decreasing pion mass, the reader will notice that the form factor for 300 MeV pions already lies below the experimental data, and thus the pole mass that would be obtained from a VMD fit to the lattice data would be considerably lower than the physical ρ mass. In view of the clear discrepancy with the experimental situation, we do not attempt a chiral extrapolation to the data, and a corresponding VMD fit. This discrepancy is perhaps expected since it is known that $\mathcal{O}(a)$ scaling violations in the vector meson mass computed with Wilson fermions yield an underestimate of the mass of roughly 20% [50], the same amount needed to move the form factor points so as to lie above the continuum curve.

For our subsequent determinations of the pion form factor in unquenched QCD using the DWF data set, we

TABLE II. Simulation details for domain-wall fermion calculations on $20^3 \times 64$ dynamical MILC ASQTAD lattices at $a^{-1} \approx 1.6$ GeV. The masses of the light (ud) and strange (s) quarks used to generate the configurations are denoted by m_{ud} and m_s, respectively, while m_{val} denotes the mass used in the valence DWF propagator. The physical meson masses are those obtained from the DWF calculation.

am_{ud}	am_s	am_{val}	m_ρ (MeV)	m_π (MeV)	m_π/m_ρ	$m_\pi L$	Z_V^{loc}	$Z_V^{\mathrm{p.s.}}$
0.01	0.05	0.01	956(22)	318(3)	0.333(8)	3.97(4)	1.0714(55)	1.1098(23)
0.05	0.05	0.05	955(19)	602(5)	0.630(12)	7.68(6)	1.0890(55)	1.0835(37)
0.05	0.05	0.081	1060(14)	758(5)	0.715(10)	9.66(6)	1.1199(14)	1.0833(13)

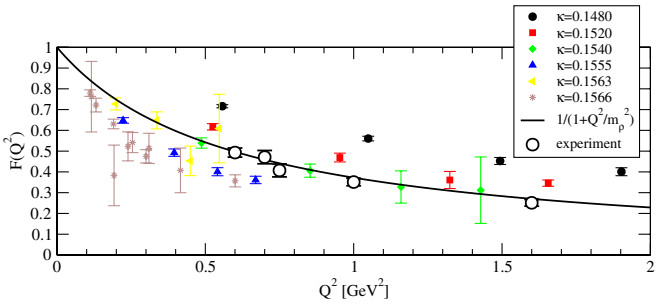

FIG. 3 (color online). Results for the pion form factor as a function of Q^2 for each of the available κ values together with experimental determinations. The line shows the VMD form, using the experimental determination of the ρ mass. Also shown as the open circles is a recent experimental determination [8], illustrating the extent to which the VMD form describes the data.

spent a substantial amount of effort in extending the calculation to higher values of Q^2 than those attained in the quenched computation. Thus we required the extraction of the pion energies and amplitudes at relatively large momenta; note that the largest attainable momenta is constrained by the fineness of the lattice spacing. In the continuum limit, the pion dispersion relation should approach the continuum one,

$$E_\pi(\boldsymbol{p})^2 = \boldsymbol{p}^2 + E_\pi(0)^2. \tag{19}$$

At a nonzero lattice spacing, a study of free lattice bosons suggests the lattice dispersion relation

$$\hat{E}(\hat{\boldsymbol{p}})^2 = \hat{\boldsymbol{p}}^2 + \hat{E}_\pi(0)^2 \tag{20}$$

where $\hat{E}$ and $\hat{p}$ are the ''lattice'' energy and momentum, respectively,

$$\hat{E} = 2\sinh\left(\frac{E}{2}\right), \qquad \hat{p}_x = 2\sin\left(\frac{p_x}{2}\right). \tag{21}$$

Equations (19) and (20) agree in the small-momentum limit. In Fig. 4, we show the measured lattice energies against the lattice momenta at each of our quark masses, together with lines representing the continuum and lattice dispersion relations. We see that both dispersion relations provide a reasonable representation of the data, although there may be a slight flattening of the data against the continuum curve at higher momenta. These results suggest that directly fitting all the data to either dispersion relation, thereby reducing the number of fit parameters needed to

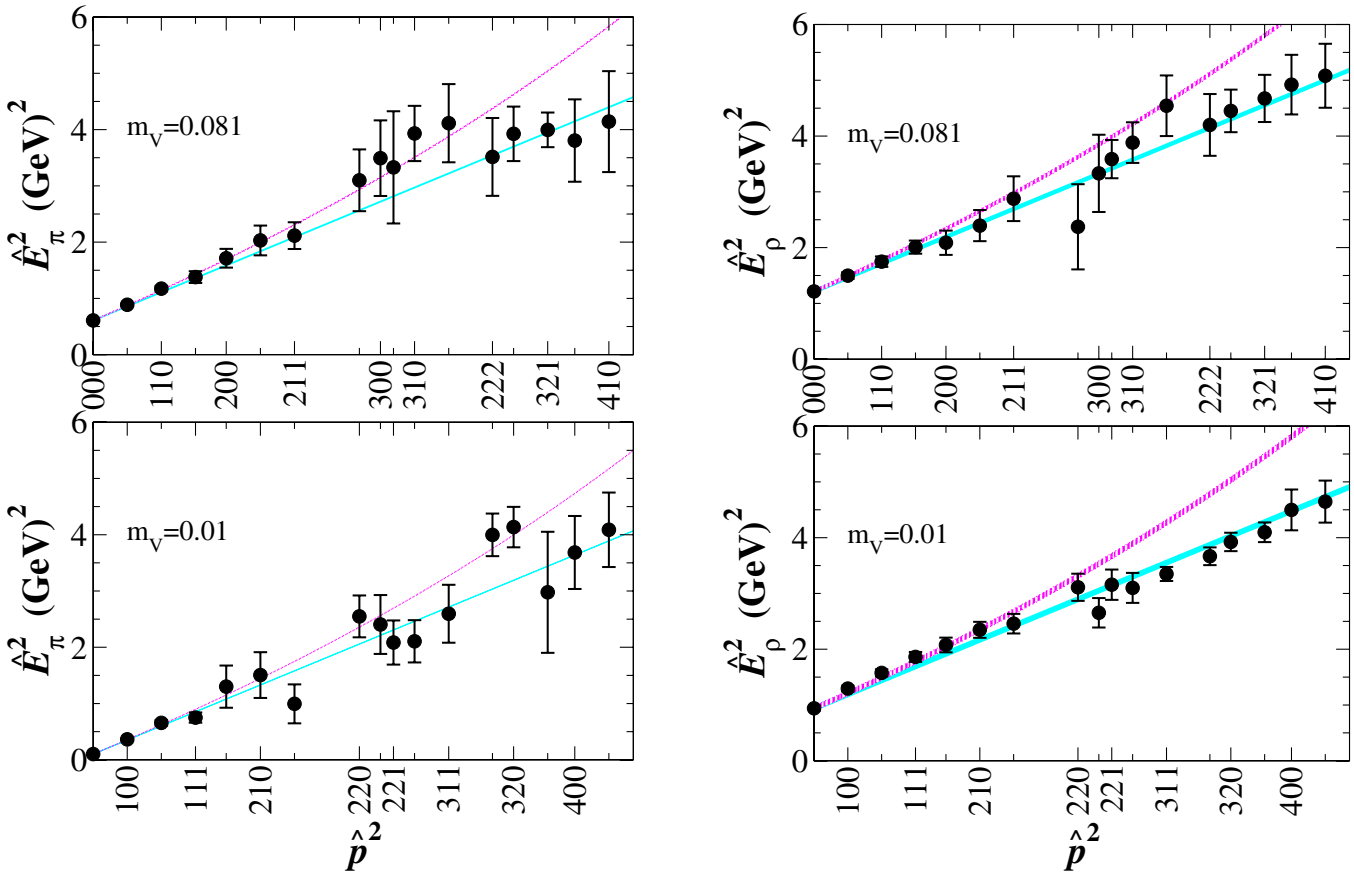

FIG. 4 (color online). Pion (left) and rho meson (right) dispersion relation vs continuum (upper) and lattice (lower) expectations curves.

extract the form factor, may improve the relative signal-to-noise of the remaining parameters. This may help dramatically in the ratio method, where the only fit parameters are the form factor and the energies.

In the fitting method, one must reliably extract not only the energies at high momenta, but also the amplitudes. In Fig. 5 we present the four amplitudes of Eqs. (11)–(14) that we estimate from the four two-point correlators we measure: smeared-smeared and smeared-local for both pseudoscalar-pseudoscalar and axial-axial operators. In the fitting procedure, all four correlators are constrained to have the same energy. From the figure, we can see that our expectations of $Z_L^{(1)} \propto \text{const}$ and $Z_L^{(2)}(\boldsymbol{p}) \propto E_\pi(\boldsymbol{p})$ are consistent with the data. We can also see from $Z_S^{(1)}(\boldsymbol{p} = 0)$ that the smeared pseudoscalar operator has a strong overlap with the zero momentum pion relative to the axial-vector operator.

We plot in Fig. 5 just the relative error estimates for the amplitudes. This clearly demonstrates that the statistical noise inherent in a particular source or sink operator need not be correlated with the magnitude of the amplitude. In particular, we see that beyond the few smallest momenta, the pseudoscalar and axial-vector amplitudes are of the same order, but the inherent noise of the pseudoscalar operator is unacceptably large for higher momenta.

Our final DWF results for the form factor are obtained from the local vector current using the lattice dispersion relation, and the ratio method described above. We also computed the form factor from the point-split vector current with comparable accuracy, but found the local and point-split results to be so correlated that combining the results proved no more accurate, suggesting that $\mathcal{O}(a^2)$ discretization errors in the currents are too small to be statistically resolved. The form factor at two of our dynamical pion masses are shown in Fig. 6, together with fits of the data to the monopole form of Eq. (1). The shaded regions correspond to jackknife error bands and the central values for the pole masses are given in the legend. The data in Fig. 6 were computed with a pseudoscalar pion sink operator fixed at momentum $\boldsymbol{p}_f = (1, 0, 0)$. Table III summarizes the fits for all available combinations of m_{val} and $\boldsymbol{p}_f$.

One common criticism of the ratio method is that it is difficult to incorporate possible excited state contributions. So, we also performed the analysis using the same fitting method described earlier, where we also ignored contribu-

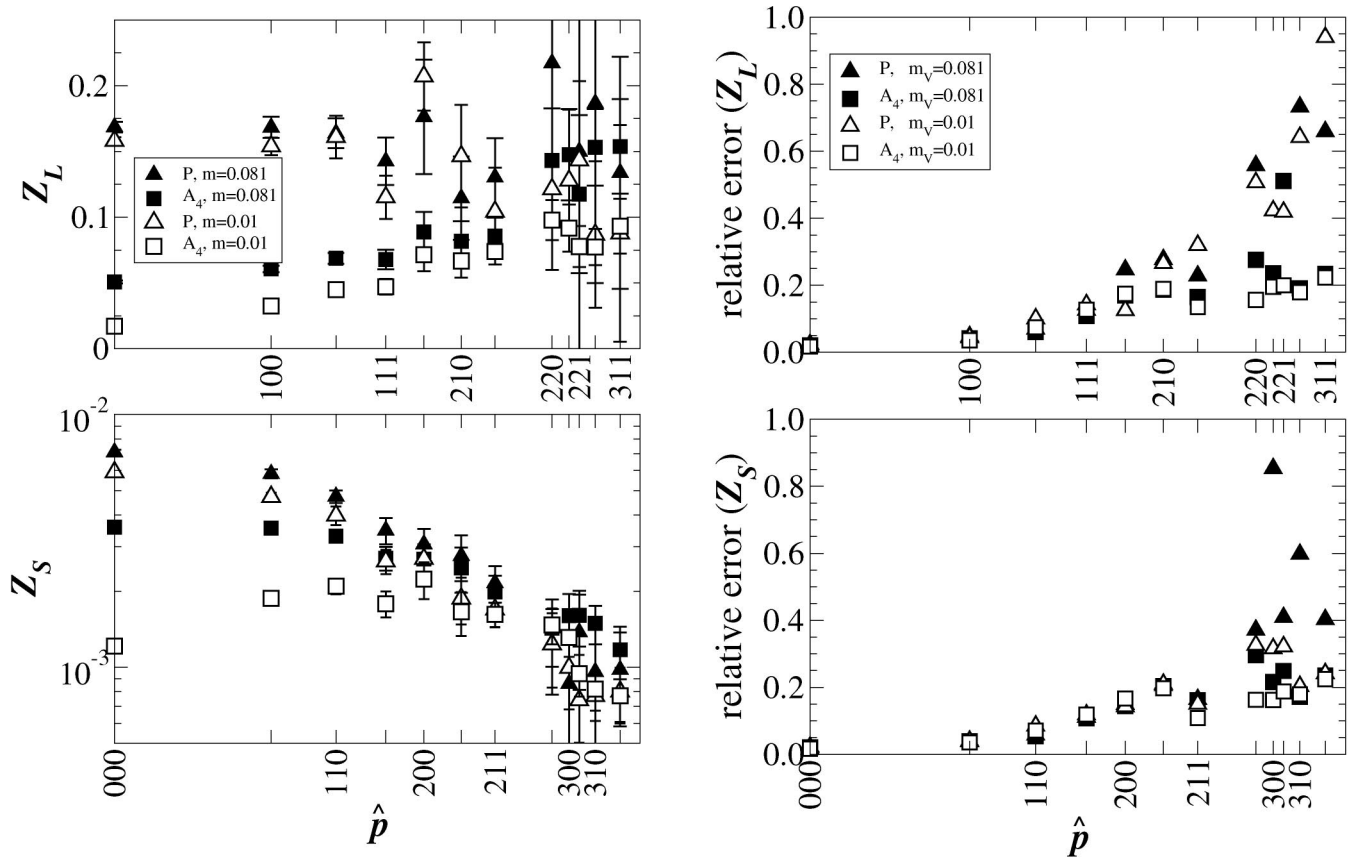

FIG. 5. Results for the local (L) and smeared (S) pseudoscalar (▲, △) and axial-vector (■, □) pion source amplitudes $Z_A^{(i)}(\boldsymbol{p})$ used in this study.

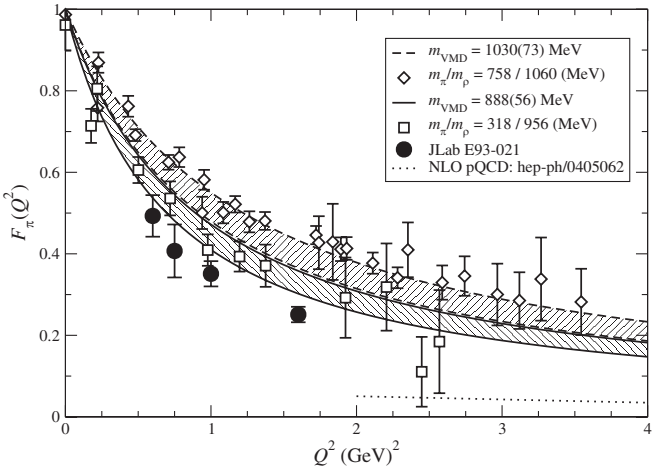

FIG. 6. Pion electromagnetic form factor for fixed sink momentum $\boldsymbol{p}_f = (1, 0, 0)$ computed by the ratio method [39,40] and imposing the lattice dispersion relation, Eq. (20). Shaded regions are jackknife error bands for VMD fit.

tions from excited states. We expect, if excited state contributions were important, we should see significant systematic differences between the ratio and fitting methods. The two methods produced results of comparable accuracy and no systematic deviations were observed.

We obtain a value of the pole mass in the chiral limit by performing an unconstrained linear extrapolation of the two most reliable data points for m_{VMD}, at $m_{\mathrm{val}} = 0.01$ and 0.081 with $\boldsymbol{p}_f = (1, 1, 0)$. This yields $m_{\mathrm{VMD}} = 0.868(65)$ GeV in the zero quark mass limit. From this we estimate the mean square charge radius of the pion to be $\langle r^2\rangle_{\mathrm{VMD}} = 0.310(46)$ fm^2, which is significantly below the experimental value of $\langle r^2\rangle_{\mathrm{expt}} = 0.439(8)$ fm^2. More dynamical quark masses, particularly lighter ones, will be needed to perform a proper chiral extrapolation.

We were unable to compute statistically significant form factors with the same pseudoscalar sink operator for $m_{\mathrm{val}} = 0.01$ and $\boldsymbol{p}_f = (1, 1, 0)$ by the ratio method, apparently due to the poor signal-to-noise inherent in the overlap of the chosen sink operator with the higher momentum state. For $m_{\mathrm{val}} = 0.01$ and $\boldsymbol{p}_f = (0, 0, 0)$ the signal was rather better but 51 sequential propagators were too few to allow for a stable fit to the VMD ansatz. We expect that an axial-vector sink operator would be a better choice for future calculations at nonzero sink momentum. Some of us are also extending our group-theoretical construction of extended baryon operators [51–55] to include mesonic quantum numbers.

TABLE III. Results of fit of form factor data to the VMD monopole ansatz of Eq. (1).

am_{val}	$\boldsymbol{p}_f$	m_{VMD} (GeV)	χ^2/d.o.f.	d.o.f.	N_{confs}
0.01	(0,0,0)	···	···	···	51
	(1,0,0)	0.888(56)	1.37(72)	13	251
	(1,1,0)	0.30(20)	1.7(1.2)	11	106
0.05	(0,0,0)	1.278(87)	2.8(1.3)	20	104
0.081	(0,0,0)	1.192(93)	3(17)	15	49
	(1,0,0)	1.030(73)	2.1(1.7)	22	70
	(1,1,0)	1.022(87)	3.6(2.2)	23	73

V. CONCLUSIONS

From our quenched Wilson form factor results, we find that both the ratio method and the fitting method are useful tools for computing the pion form factor. Each method has different systematic errors, so the extent to which both agree should give confidence that the systematic errors are small and well understood. A comparison of the Wilson form factor results with the experimental pion form factor data suggests that the former have large, and expected, discretization errors. Thus the use of an improved fermion action would seem essential if contact is to be made with the experimental situation.

Domain-wall fermions are free of $\mathcal{O}(a)$ discretization uncertainties to the extent that any residual mass is eliminated. Thus in our subsequent dynamical fermion study, we employed domain-wall fermions for the valence quarks, computed on ASQTAD lattices. From a careful analysis of the pion spectrum, we recognize the importance of using a large basis of pion operators so that we can identify at least one operator at each pion momentum whose overlap with the pion has a reasonable signal-to-noise ratio. The local axial-vector operator appears to be a better choice than the pseudoscalar operator for fitting higher momentum states since its overlap with a given state increases in proportion with the pion energy and without any degradation of the signal-to-noise ratio.

Our analysis enables us to obtain the pion form factor for a pion mass approaching 300 MeV at a range of Q^2 commensurate with the current experimental program. We find that a VMD form provides a faithful description of the pion form factor over this Q^2 range, and an unconstrained linear fit yields $m_{\mathrm{VMD}} = 0.868(65)$ GeV in the chiral limit.

A comparison between the full-QCD and quenched-QCD results is clouded by the large discretization errors indicated in the latter. While this issue could be investigated through a quenched DWF calculation, such a computation would be as demanding as the hybrid ASQTAD sea-quark/domain-wall valence quark computation presented here, given the availability of the full-QCD gauge configurations. It is this hybrid approach that enables us to make our first forays into full-QCD studies of pion structure at light quark masses.

Given our existing analysis framework and the propagators and sequential propagators that we have already computed, we can also compute the $\rho^+ \to \gamma\pi^+$ transition

form factor. This analysis will be completed in the near future.

ACKNOWLEDGMENTS

This work was supported in part by the Natural Sciences and Engineering Research Council of Canada and in part by DOE Contract No. DE-AC05-84ER40150 Modification No. M175, under which the Southeastern Universities Research Association (SURA) operates the Thomas Jefferson National Accelerator Facility. Computations were performed on the 128-node and 256-node Pentium IV clusters at JLab and on other resources at ORNL, under the auspices of the National Computational Infrastructure for Lattice Gauge Theory, a part of U.S. DOE's SciDAC program. We are grateful to the MILC Collaboration for making available their configurations.

[1] N. Isgur and C. H. Llewellyn Smith, Phys. Rev. Lett. **52**, 1080 (1984).
[2] W. G. Holladay, Phys. Rev. **101**, 1198 (1956).
[3] W. R. Frazer and J. R. Fulco, Phys. Rev. Lett. **2**, 365 (1959).
[4] W. R. Frazer and J. R. Fulco, Phys. Rev. **117**, 1609 (1960).
[5] S. R. Amendolia *et al.* (NA7 Collaboration), Nucl. Phys. **B277**, 168 (1986).
[6] C. J. Bebek *et al.*, Phys. Rev. D **17**, 1693 (1978).
[7] P. Brauel *et al.*, Z. Phys. C **3**, 101 (1979).
[8] J. Volmer *et al.* (The Jefferson Lab F_π Collaboration), Phys. Rev. Lett. **86**, 1713 (2001).
[9] F. Gutbrod and G. Kramer, Nucl. Phys. **B49**, 461 (1972).
[10] M. Guidal, J. M. Laget, and M. Vanderhaeghen, Nucl. Phys. **A627**, 645 (1997).
[11] M. Vanderhaeghen, M. Guidal, and J. M. Laget, Phys. Rev. C **57**, 1454 (1998).
[12] H. P. Blok, G. M. Huber, and D. J. Mack, nucl-ex/0208011.
[13] P. Maris and P. C. Tandy, Phys. Rev. C **62**, 055204 (2000).
[14] F. Cardarelli, E. Pace, G. Salme, and S. Simula, Phys. Lett. B **357**, 267 (1995).
[15] F. Iachello, Eur. Phys. J. **A19**, Suppl. 1, 29 (2004).
[16] F. Iachello and Q. Wan (to be published).
[17] S. J. Brodsky and G. R. Farrar, Phys. Rev. Lett. **31**, 1153 (1973).
[18] S. J. Brodsky and G. R. Farrar, Phys. Rev. D **11**, 1309 (1975).
[19] G. R. Farrar and D. R. Jackson, Phys. Rev. Lett. **43**, 246 (1979).
[20] A. V. Radyushkin, hep-ph/0410276.
[21] A. V. Efremov and A. V. Radyushkin, in *Proceedings of the XIX International Conference on High Energy Physics, Tokyo, Japan, 1978*, edited by S. Homma (Physical Society of Japan, Tokyo, 1979).
[22] A. V. Efremov and A. V. Radyushkin, Theor. Math. Phys. (Engl. Transl.) **42**, 97 (1980).
[23] A. V. Efremov and A. V. Radyushkin, Phys. Lett. B **94**, 245 (1980).
[24] D. R. Jackson, Ph.D. thesis, California Institute of Technology, 1977.
[25] G. P. Lepage and S. J. Brodsky, Phys. Lett. B **87**, 359 (1979).
[26] N. G. Stefanis, W. Schroers, and H.-C. Kim, Phys. Lett. B **449**, 299 (1999).
[27] N. G. Stefanis, W. Schroers, and H.-C. Kim, hep-ph/9812280.
[28] N. G. Stefanis, W. Schroers, and H.-C. Kim, Eur. Phys. J. C **18**, 137 (2000).
[29] A. P. Bakulev, K. Passek-Kumericki, W. Schroers, and N. G. Stefanis, Phys. Rev. D **70**, 033014 (2004).
[30] S. J. Brodsky, C.-R. Ji, A. Pang, and D. G. Robertson, Phys. Rev. D **57**, 245 (1998).
[31] G. Martinelli and C. T. Sachrajda, Nucl. Phys. **B306**, 865 (1988).
[32] T. Draper, R. M. Woloshyn, W. Wilcox, and K.-F. Liu, Nucl. Phys. **B318**, 319 (1989).
[33] J. van der Heide, M. Lutterot, J. H. Koch, and E. Laermann, Phys. Lett. B **566**, 131 (2003).
[34] Y. Nemoto (RBC Collaboration), Nucl. Phys. B Proc. Suppl. **129**, 299 (2004).
[35] A. M. Abdel-Rehim and R. Lewis, Nucl. Phys. B Proc. Suppl. **140**, 299 (2005).
[36] J. van der Heide, J. H. Koch, and E. Laermann, Phys. Rev. D **69**, 094511 (2004).
[37] J. van der Heide, J. H. Koch, and E. Laermann, Few-Body Syst. **36**, 119 (2005).
[38] A. M. Abdel-Rehim and R. Lewis, Phys. Rev. D **71**, 014503 (2005).
[39] F. D. R. Bonnet, R. G. Edwards, G. T. Fleming, R. Lewis, and D. G. Richards, Nucl. Phys. B Proc. Suppl. **129**, 206 (2004).
[40] F. D. R. Bonnet, R. G. Edwards, G. T. Fleming, R. Lewis, and D. G. Richards (LHP Collaboration), Nucl. Phys. B Proc. Suppl. **128**, 59 (2004).
[41] R. Frezzotti and G. C. Rossi, Nucl. Phys. B Proc. Suppl. **128**, 193 (2004).
[42] C. W. Bernard *et al.*, (MILC Collaboration), Phys. Rev. D **64**, 054506 (2001).
[43] J. W. Negele *et al.* (LHP Collaboration), Nucl. Phys. B Proc. Suppl. **128**, 170 (2004).
[44] D. B. Renner *et al.* (LHP Collaboration), Nucl. Phys. B Proc. Suppl. **140**, 255 (2005).
[45] J. W. Negele *et al.* (LHP Collaboration), Nucl. Phys. B Proc. Suppl. **129**, 910 (2004).
[46] W. Schroers *et al.* (LHP Collaboration), Nucl. Phys. B Proc. Suppl. **129**, 907 (2004).
[47] P. Hägler *et al.* (LHP Collaboration), Eur. Phys. J. A **24S1**, 29 (2005).
[48] A. Hasenfratz and F. Knechtli, Phys. Rev. D **64**, 034504

(2001).
[49] C. Aubin *et al.*, Phys. Rev. D **70**, 094505 (2004).
[50] R. G. Edwards, U. M. Heller, and T. R. Klassen, Phys. Rev. Lett. **80**, 3448 (1998).
[51] R. Edwards *et al.* (LHP Collaboration), Nucl. Phys. B Proc. Suppl. **129**, 236 (2004).
[52] S. Basak *et al.* (LHP Collaboration), Nucl. Phys. B Proc. Suppl. **129**, 209 (2004).
[53] S. Basak *et al.* (LHP Collaboration), Nucl. Phys. B Proc. Suppl. **128**, 186 (2004).
[54] S. Basak *et al.* (LHP Collaboration), Nucl. Phys. B Proc. Suppl. **140**, 281 (2005).
[55] S. Basak *et al.* (LHP Collaboration), Nucl. Phys. B Proc. Suppl. **140**, 287 (2005).